KRONOS FUSION ENERGY

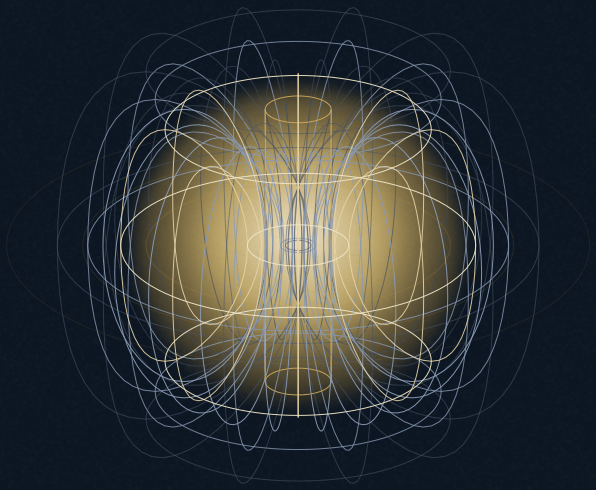

PAPER 2.50 · THE KRONOS 2026 SERIES

Tritium Permeation-Barrier Coatings for a Compact Spherical-Tokamak Breeder: The Liquid-Lithium-over-Tin Wall-Chemistry Choice

The tritium a breeder keeps out of its structure is tritium it keeps in its fuel cycle, and the two decisions that set that balance both live at the first wall: which liquid…

Read it live — 3-D model · physics validator · film series

BY P I FORDOFFICIAL VERSION: HTTPS://WWW.KRONOSFUSIONENERGY.COM/PUBLICATIONS/TRITIUM-PERMEATION-BARRIER-COATINGS-FOR-A-COMPACT-SPHER.HTML AND G L KULCINSKI

2026 · EDITORIAL EDITION

THE OFFICIAL RECORD

What this document is, and how to read its numbers

This is a combined editorial. It gathers, in one volume, the two design studies Kronos Fusion Energy released in 2026 — a compact spherical-tokamak tritium/helium-3 breeder and a deuterium–helium-3 tandem-mirror generator — together with the intellectual-property estate, the people, and, in the internal edition, the full commercial case. The scientific text is the same text that appears in the arXiv preprints and the journal submissions; the editorial adds the apparatus a reader needs to hold the whole program at once, and nothing in the physics is altered to fit it.

THE HONESTY STANCE IS THE ASSET

Every headline quantity carries an **evidence class** — DERIVED · RECOMPUTED · MEASURED · REQUIREMENT — and, where a number is a modelled extrapolation rather than a demonstrated value, it is labelled as such and its downside is shown next to it. Several quantities in the underlying corpus moved after first publication; where a value has been withdrawn or restated, the record says so plainly. This is deliberate: a diligence team will find the load-bearing assumptions, so the document surfaces them first.

TWO EDITIONS

This volume is issued in two editions. The **public edition** (light) carries the physics and the design only — no dollar, price, or per-kilogram figure appears anywhere in it. The **internal edition** (dark) adds the economics, the funding architecture, and the defense-commercial analysis, and is marked *Confidential* accordingly; it is not for public distribution. Where the commercial case rests on a modelled assumption rather than a demonstrated one, it is labelled as such and its downside is shown alongside it, on the same terms as the physics.

TITLE	The Kronos Fleet — Hyperion · Aegis · MetroVolt: A Combined Design & Commercialization Study
AUTHOR	Priyanca Ford, Founder & CEO, on behalf of Kronos Fusion Energy
EDITION	2026 Combined Editorial · first issue
COMPANION WORKS	The five-paper arXiv drop — (1) Breeder, (2) Burner, (3) REBCO magnet & tape, (4) Direct Energy Conversion, (5) AI/ML/Quantum control — with matching numbered Zenodo deposits, plus the IOP journal and IAEA-FEC submissions. Patents were filed before the drop.
NAMING	Hyperion = the breeder; Aegis (defense) and MetroVolt (data-center) = one generator in two housings. Internal mode letters (D1, L) do not appear on public surfaces.
STATUS	Conceptual design & simulation study. Nothing herein is a construction commitment.

HOW TO READ THIS VOLUME

The fleet at a glance, and the way its numbers are marked

This volume opens with *Orientation*, presents the five research papers as a bound sequence, and closes with the *Apparatus*. *Foundations* sets out the three general results both machines rest on. *Paper One* is the Hyperion breeder; *Paper Two* the Aegis / MetroVolt generator; *Papers Three, Four and Five* are the enabling science — high-field REBCO magnets and tape, direct energy conversion, and the AI / ML / quantum control stack. A *Digital Twin & 3-D Model* part follows, then the *Environmental* profile. The *Economics* and levelized cost and the *Business Case* and diligence record appear in the internal edition only; the *Simulations* proof record and the Apparatus — patent portfolio, team, limitations, and sources — close both editions.

THE FLEET AT A GLANCE

	HYPERION	AEGIS	METROVOLT
Role	Strategic-isotope foundry	Defense installation power	Campus power
Machine	**Spherical tokamak**	**Tandem mirror**	**Tandem mirror**
Fuel	Deuterium–tritium	Deuterium–helium-3	Deuterium–helium-3
Delivers	Tritium · ^{3}He · 14 MeV n	Resilient installation power	Firm campus power
Physics bar	**Fusion gain only**	Closure (gates named)	Closure + lunar ^{3}He
In the fleet	Breeds the fuel	Proves the generator	Commercial destination

HOW THE NUMBERS ARE MARKED

Every headline quantity carries an evidence class — DERIVED from first principles, RECOMPUTED from raw data, MEASURED in hardware, or a REQUIREMENT yet to be met. Financial figures carry a case label and are confined to the internal (confidential) edition. Values that moved after first publication are shown as withdrawn or restated rather than quietly changed. A capability you can evaluate is one whose limits are on the page.

ABSTRACT

Tritium Permeation-Barrier Coatings for a Compact Spherical-Tokamak Breeder: The Liquid-Lithium-over-Tin Wall-Chemistry Choice

The tritium a breeder keeps out of its structure is tritium it keeps in its fuel cycle, and the two decisions that set that balance both live at the first wall: which liquid metal, if any, faces the plasma, and what barrier protects the structure behind it. We resolve both for the Hyperion compact spherical-tokamak breeder ($P_{\mathrm{fus}} = 85.04\,MW$, $I_p = 9.66\,MA$, $Q = 3.076$, negative triangularity $\delta = -0.30$, $B_0 = 8\,T$, elongation $\kappa = 2.0$, major radius $R_0 = 1.20\,m$, aspect ratio $A = 2.5$, centrepost peak field $16.84\,T$). We formalise the coupled fuel-cycle and first-wall transport problem — a McNabb–Foster diffusion–trapping system with Sieverts chemical-potential continuity across a tungsten/steel interface, closed by an implantation source and recombination boundaries — and solve it by finite element (FESTIM/FEniCS) on the actual 0.5 mm W + 2 mm Eurofer97 stack as part of the Kronos NVIDIA GPU high-performance-computing campaign. The steady permeation flux is $5.16 \times 10^{14}\ \mathrm{T\,m^{-2}s^{-1}} \approx 0.082\,g\,\mathrm{T\,m^{-2}fpy^{-1}}$, only 0.52–0.60 % of the implanted flux, with ∼99.4 % re-emitted; the stack is tungsten-diffusion-limited because the tungsten-to-steel solubility partition is $\sim 2 \times 10^{-5}$, and the finite-element result reproduces the analytic two-layer series-resistance limit to seven significant figures. Being diffusion-limited, the loss flux is temperature-independent and linear in load, so for a $\sim 100\,m^2$ wall it is a bounded ~ 8–$10\,g\,\mathrm{T\,fpy^{-1}}$ holdup against a kilogram-scale surplus. On the liquid-metal axis, pure lithium retains tritium about 6.7 orders of magnitude more strongly than tin — and 4.6 orders more than lead–lithium — because its equilibrium tritium partial pressure, the driving pressure for permeation, is far lower; the resulting breakthrough buffer is of order 7000 h and the choice of the plasma-facing liquid is lithium. Behind it, an oxide barrier screen ranks $\mathrm{Al_2O_3}$ (PRF $\sim 10^3$) > $\mathrm{Er_2O_3}$ ($\sim 3 \times 10^2$) > TiC > TiN, and an yttrium hot-trap ($\Delta G = -83$ to $-97\,kJ/mol$) with a 92 % cold-trap closes the recovery loop; the same lithium loop hands the exhaust a 2.8–6.7 MW/m^2 flowing-film surface. One material choice therefore protects the fuel cycle, admits a barrier, and self-heals the exhaust at once.

Open-access deposit (code & data, CC BY 4.0): DOI 10.5281/zenodo.22645870 · Zenodo community *kronos_fusion_energy*. Explore it live: interactive 3-D model · physics validator.

Keywords: tritium permeation · permeation barrier · liquid lithium · liquid tin · PbLi · FESTIM · McNabb--Foster · Sieverts law · first wall · flowing-lithium divertor · spherical-tokamak breeder

CONTENTS

Table of Contents

NOMENCLATURE

Symbols, units, and the names of things

Q	plasma (fusion) gain, P_{fus}/P_{aux}
Q_E	engineering gain, net electric out / recirculating in
H_{98}	confinement enhancement over the IPB98(y,2) scaling
Z_{eff}	effective ion charge
c_{ee}	electron–electron bremsstrahlung leading coefficient, 2.120022 (exact)
τ_E	energy confinement time
I_p	plasma current
R_0, a	major radius, minor radius
κ, δ	elongation, triangularity
β_N	normalized plasma beta (Troyon-normalized)
TBR	tritium breeding ratio
DEC	direct energy conversion
CF	plant capacity factor (availability)
FOAK / NOAK / BOAK	first / n^{th} / best of a kind
Hyperion	the ST breeder (internal: Mode D2)
Aegis	the generator, defense/installation housing (internal: Mode M)
MetroVolt	the generator, data-center housing (Mode M)

§ 1

Introduction

TRITIUM BOOKKEEPING DECIDES A BREEDER

A deuterium–tritium breeder lives or dies on tritium bookkeeping. Tritium does not exist in nature in usable quantity; a fusion plant must breed its own from lithium and hold the resulting inventory in surplus while it burns, decays ($t_{1/2} = 12.32$ yr), and loses a fraction of it to structure, coolant and processing. The margin is narrow. Global analyses of the D–T fuel cycle place the required breeding ratio uncomfortably close to unity once realistic losses, reserves and doubling times are folded in, and identify the loss and holdup terms — not the raw breeding reaction — as the levers that decide self-sufficiency [1,2,3]. Every atom that permeates into structure is subtracted from that margin; every atom held on a plasma-facing surface is a driving pressure a barrier must hold back and a safety-relevant inventory that must be accounted. For the Hyperion breeder, whose whole thesis is to run as a strategic-materials and tritium platform rather than a power plant [28], the first-wall tritium architecture is therefore not a detail but a load-bearing part of the design.

Two decisions dominate that architecture, and both live at the first wall. The first is the plasma-facing liquid: a flowing liquid-metal surface removes the brittle-solid failure modes of a refractory wall and self-heals under transient heat loads, but it introduces a dissolved tritium inventory whose equilibrium partial pressure drives permeation and sets the tritium hazard of the loop. The candidate liquids — lithium, tin, and lead–lithium — are not close on this axis. The second is the barrier stack behind the liquid: the coating and getter chemistry that divides the permeation flux and routes the residue into a measured recovery stream.

PRIOR ART

Hydrogen transport in fusion first-wall materials is a mature quantitative science. Diffusion and solubility of hydrogen isotopes in tungsten were fixed by Frauenfelder's classic measurements [4], and trapping at intrinsic and damage sites has since been characterised in detail [8,9]. The reduced-activation ferritic–martensitic (RAFM) steel Eurofer97, the reference structural material behind the armour, has a well-measured permeability and trap spectrum [6,7]. The governing diffusion–trapping description is the McNabb–Foster model [5], and the implantation-driven, recombination-limited/diffusion-limited permeation regimes are the Pick–Sonnenberg framework [10] implemented in verified tritium-migration codes such as TMAP [11] and, more recently, the open-source finite-element code FESTIM [12,13] built on the FEniCS project [14]. Tritium permeation barriers — principally dense Al_2O_3 and Er_2O_3 oxide layers — have been reviewed and measured with permeation-reduction factors (PRF) spanning 10^2–10^4 [15,16,17,18,19]. On the liquid-metal side, flowing lithium has been run as a plasma-facing material on CDX-U, LTX and NSTX [20,21], the lithium vapour-box divertor concept has been developed to cap the strike-point heat flux [22], and liquid tin and tin–lithium have been proposed where lithium's tritium inventory is judged too aggressive [23,24]. What has not been done is to settle both first-wall decisions *jointly and quantitatively for one machine* — to compute the permeation loss term of the actual armour/steel stack rather than assume it, and to rank the liquids on the single figure of merit that the fuel cycle cares about — and to show that the two choices reinforce each other.

CONTRIBUTION

This paper does exactly that for Hyperion (figure 1). We (i) write the coupled fuel-cycle and first-wall transport problem as a formal system of equations (§2), including the diffusion-limited series-resistance limit that the finite-element solve must recover and the liquid-metal driving-pressure model that ranks the facing liquids; (ii) solve the first-wall permeation problem by finite element on the real stack as part of the Kronos NVIDIA GPU HPC campaign, with the codes, mesh, solver and verification stated explicitly (§3); (iii) present the results — the liquid-metal ranking, the computed permeation flux and its temperature-independence, the retained inventory and breakthrough time, the barrier and getter ladder, and the divertor co-benefit — across eight data figures and three tables (§4); (iv) benchmark those numbers against the published permeation, barrier and liquid-lithium literature (§5); and (v) state the single open gate honestly (§6). Every quantitative claim traces to a frozen result in the Kronos Physics De-Risking Register [34]: the finite-element permeation solve is serial BR-L2-A25, the liquid-metal and barrier chemistry screen is BR-SX-03, and the flowing-lithium divertor thermofluids are HX-16/BR-CX-25. Where the result feeds a companion study — the tritium breeding ladder [29], the real-time tritium-accountancy twin [30], the flowing-lithium vapour-box divertor [31], the RAFM-steel qualification [32], or the first-wall neutron-damage lifetime [33] — the link is cited inline.

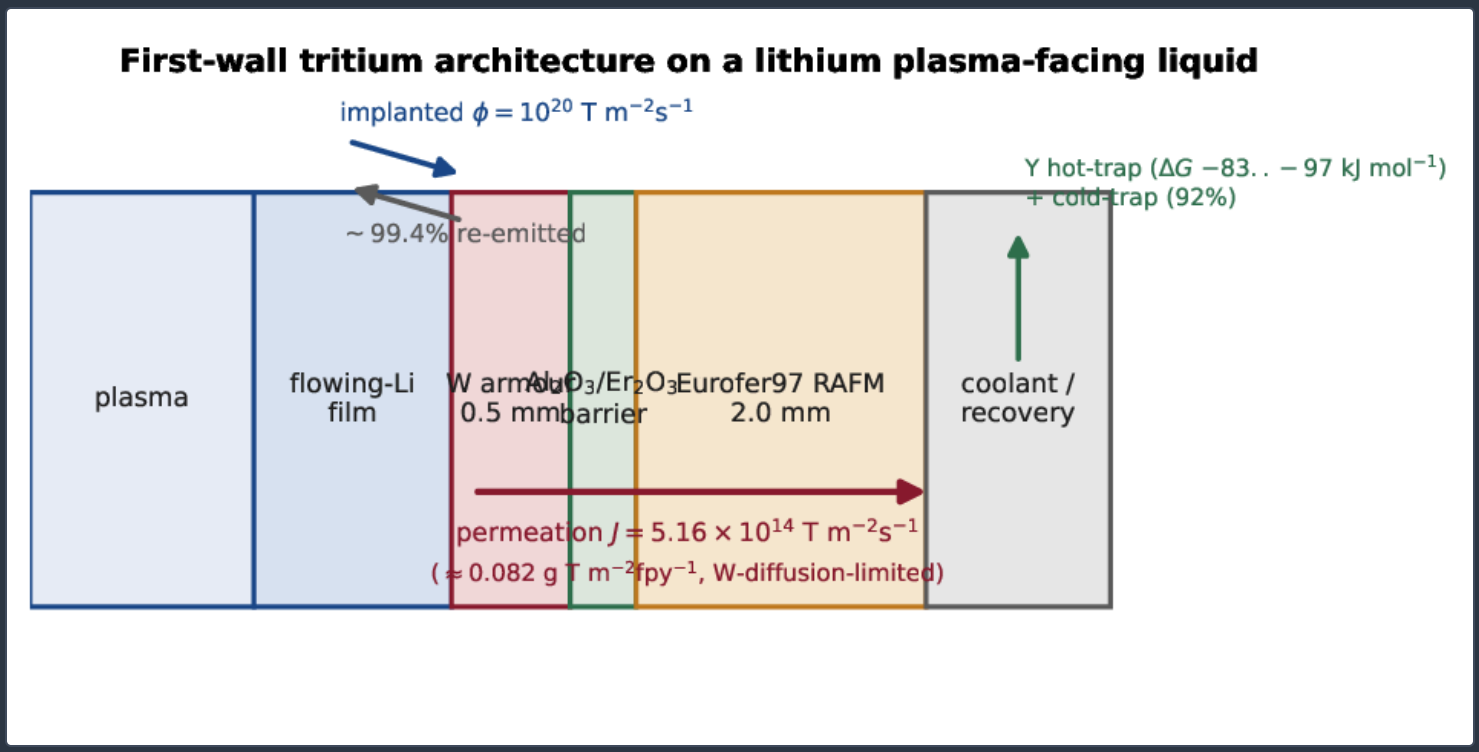

(Schematic.) The first-wall tritium architecture on a lithium plasma-facing liquid. Tritium is implanted from the plasma at $\varphi = 1e20\ /m^2s$; $\sim 99.4\,\%$ re-emits, and the residue permeates the 0.5 mm W + 2 mm Eurofer stack at the tungsten-diffusion-limited flux $J = 5.16 \times 10^{14}\ \mathrm{T\,m^{-2}s^{-1}}$. A dense $\mathrm{Al_2O_3/Er_2O_3}$ barrier divides the flux and an yttrium hot-trap plus cold-trap recover it into a measured stream. The elements are drawn to indicate sequence and function, not to scale.

§ 2

Governing equations and the formal problem

THE FUEL-CYCLE BALANCE AND WHERE PERMEATION ENTERS

The plant-level quantity the first-wall calculation must feed is the tritium inventory $I_T(t)$, which evolves as

$$\frac{\mathrm{d}I_T}{\mathrm{d}t} = \dot{N}_{\mathrm{bred}} - \dot{N}_{\mathrm{burn}} - \lambda_T I_T - \dot{N}_{\mathrm{loss}}, \qquad \lambda_T = \frac{\ln 2}{t_{1/2}}, \quad t_{1/2} = 12.32\ \mathrm{yr},$$

with breeding source $\dot{N}_{\mathrm{bred}} = \mathrm{TBR}\,\dot{N}_{\mathrm{burn}}$, burn rate $\dot{N}_{\mathrm{burn}}$, radioactive decay $\lambda_T I_T$, and an aggregate loss $\dot{N}_{\mathrm{loss}}$. Self-sufficiency is the requirement that the net breeding gain clear unity once a fractional loss ε is charged against it,

$$\Lambda \;\equiv\; \mathrm{TBR}\,(1-\varepsilon) - 1 \;\geq\; 0.$$

First-wall permeation is one contribution to ε: integrating the permeation flux J over the wall area A gives a loss rate $\dot{N}_{\mathrm{loss}}^{\mathrm{perm}} = \int_A J\,\mathrm{d}A$, so the entire task of this paper is to compute J from first principles and bound its contribution to ε. Everything below serves equation (2).

DIFFUSION–TRAPPING TRANSPORT IN THE WALL

Inside the solid, mobile tritium of concentration $c_{\mathrm{m}}(\quad x,t)$ obeys a diffusion equation coupled to a set of trap populations $c_{t,i}$ through the McNabb–Foster kinetics [5]:

$$\frac{\partial c_{\mathrm{m}}}{\partial t} = \nabla\cdot\big(D(T)\,\nabla c_{\mathrm{m}}\big) + S(\quad x,t) - \sum_i \frac{\partial c_{t,i}}{\partial t},$$

$$\frac{\partial c_{t,i}}{\partial t} = k_i(T)\,c_{\mathrm{m}}\left(n_i - c_{t,i}\right) - p_i(T)\,c_{t,i},$$

where $D(T) = D_0\exp(-E_D/k_BT)$ is the Arrhenius diffusivity, n_i the density of trap type i, and the trapping and detrapping rate coefficients are

$$k_i(T) = \frac{D(T)}{\lambda^2 N}, \qquad p_i(T) = \nu_0\exp\!\Big(-\frac{E_{p,i}}{k_BT}\Big),$$

with λ the lattice spacing, N the host atomic density, ν_0 the attempt frequency, and $E_{p,i}$ the detrapping energy of trap i. For Hyperion the domain is a one-dimensional bilayer: a tungsten armour of thickness $L_{\mathrm{W}} = 0.5\,mm$ facing the plasma, bonded to a Eurofer97-class RAFM steel wall of thickness $L_{\mathrm{E}} = 2.0\,mm$. Tungsten carries two intrinsic traps ($E_p = 0.87$ and 1.00 eV, densities 1.3×10^{-3} and 4×10^{-4} atomic fraction, Ogorodnikova class [8]); the steel carries one (0.80 eV, 10^{-4} atomic fraction).

INTERFACE AND BOUNDARY CLOSURE

Across the tungsten/steel interface the transported quantity is the chemical potential, not the concentration. Under Sieverts' law each material relates its mobile concentration to the local partial pressure through $c_{\mathrm{m}} = S(T)\sqrt{p}$ with solubility $S(T) = S_0\exp(-E_S/k_BT)$, so continuity of $\sqrt{p}$ imposes the Sieverts partition

$$\left.\frac{c_{\mathrm{m}}^{\mathrm{W}}}{c_{\mathrm{m}}^{\mathrm{E}}}\right|_{\mathrm{interface}} = \frac{S_{\mathrm{W}}(T)}{S_{\mathrm{E}}(T)}.$$

This concentration jump is the mathematical origin of the tungsten-diffusion-limited behaviour derived below. At the plasma-facing surface, tritium is delivered by implantation: energetic charge-exchange and ion flux deposits a volumetric source

$$S(\quad x) = \frac{\varphi}{\sqrt{2\pi}\,\sigma}\exp\!\Big[-\frac{(x-R_p)^2}{2\sigma^2}\Big], \qquad \int_0^\infty S\,\mathrm{d}x = \varphi,$$

of range R_p and straggle σ (both $\ll L_{\mathrm{W}}$), with implanted flux $\varphi = 1e20\ /m^2s$. The two free surfaces recombine to molecular $\mathrm{T_2}$ with a second-order flux

$$J_{\mathrm{rec}} = 2\,K_r(T)\,c_{\mathrm{m}}^2,$$

and the coolant face additionally supports fast extraction ($c_{\mathrm{m}} \to 0$). The permeation flux of interest is the diffusive flux leaving the coolant face, $J = -D_{\mathrm{E}}\,\partial_x c_{\mathrm{m}}|_{x=L_{\mathrm{W}}+L_{\mathrm{E}}}$.

THE DIFFUSION-LIMITED SERIES-RESISTANCE LIMIT

Two limiting regimes follow from equations (3)–(7). When surface recombination is slow, permeation is recombination-limited and scales as $J \propto \varphi/\sqrt{K_r}$. When recombination is fast relative to diffusion — the relevant regime here, and the conservative-high case for the loss term — permeation is diffusion-limited, and the implanted atoms partition between the two faces in inverse proportion to the diffusive resistance to each. For a source implanted a depth R_p below the front surface of a membrane of total thickness L, the downstream fraction is

$$\frac{J}{\varphi} = \frac{R_p}{L},$$

a purely geometric ratio: *the diffusion-limited permeation flux is independent of temperature and linear in the implanted flux.* Equation (8) is the sharp, testable prediction the finite-element solve must reproduce, and it is the reason the loss term scales cleanly with wall load.

For pressure-driven permeation across the bilayer the same physics is expressed as a series of permeation resistances. Writing the permeability of layer j as $\Phi_j = D_j S_j$, the steady flux under a driving pressure difference is

$$J = \frac{\sqrt{p_{\mathrm{up}}} - \sqrt{p_{\mathrm{down}}}}{\mathcal{R}_{\mathrm{stack}}}, \qquad \mathcal{R}_{\mathrm{stack}} = \frac{L_{\mathrm{W}}}{\Phi_{\mathrm{W}}} + \frac{L_{\mathrm{E}}}{\Phi_{\mathrm{E}}}.$$

Because the tungsten solubility carries the larger activation energy ($E_S^{\mathrm{W}} = 1.041\,eV$ versus $E_S^{\mathrm{E}} = 0.27\,eV$), the solubility partition of equation (5) is small — $S_{\mathrm{W}}/S_{\mathrm{E}} \sim 10^{-4}$–$10^{-5}$ over 600–$800\,K$ — and the first term of $\mathcal{R}_{\mathrm{stack}}$ dominates. The stack is tungsten-diffusion-limited: the 2 mm of steel adds negligible resistance, and the series ratio $\mathcal{R}_{\mathrm{stack}}/(L_{\mathrm{W}}/\Phi_{\mathrm{W}}) \to 1$. The transient approach to this steady state is set by the Daynes–Barrer time lag; for the rate-controlling tungsten layer the breakthrough time is

$$\tau = \frac{L_{\mathrm{W}}^2}{6\,D_{\mathrm{W}}(T)}.$$

THE LIQUID-METAL DRIVING PRESSURE

The choice of plasma-facing liquid is decided by the same Sieverts physics applied to the melt. A liquid metal in contact with the plasma dissolves tritium to a concentration c^{liq} fixed by recycling; the equilibrium partial pressure it presents to the wall behind it is

$$p_{\mathrm{eq}}^{\mathrm{liq}} = \left(\frac{c^{\mathrm{liq}}}{K_S^{\mathrm{liq}}(T)}\right)^2, \qquad K_S^{\mathrm{liq}}(T) = K_{S0}\exp\!\left(-\frac{\Delta H_{\mathrm{sol}}}{k_B T}\right),$$

where K_S^{liq} is the Sieverts constant of the liquid and ΔH_{sol} its enthalpy of solution. Lithium chemically binds hydrogen isotopes (strongly negative ΔH_{sol}, tending toward LiT formation), so its K_S is large and the equilibrium pressure p_{eq} of equation (11) is orders of magnitude below that of tin, whose weak hydrogen affinity leaves a high driving pressure. Since the downstream permeation flux scales as $J \propto \sqrt{p_{\mathrm{eq}}}$ (equation 9), the *retention advantage* of one liquid over another is naturally quantified in decades of driving-pressure reduction,

$$\mathcal{A}_{\mathrm{X/Sn}} = \log_{10}\frac{p_{\mathrm{eq}}^{\mathrm{Sn}}}{p_{\mathrm{eq}}^{\mathrm{X}}},$$

and the breakthrough buffer — the time before a loop's tritium works through a protected wall — scales inversely with the driving pressure. This single figure of merit orders the candidates.

BARRIER AND GETTER FIGURES OF MERIT

A permeation barrier is a thin dense layer of much lower permeability inserted in the series stack of equation (9). Its permeation-reduction factor is the ratio of uncoated to coated flux,

$$\mathrm{PRF} = \frac{J_{\mathrm{bare}}}{J_{\mathrm{coated}}} = 1 + \frac{\mathcal{R}_{\mathrm{barrier}}}{\mathcal{R}_{\mathrm{substrate}}} \approx \frac{\Phi_{\mathrm{sub}}}{\Phi_{\mathrm{bar}}}\,\frac{L_{\mathrm{bar}}}{L_{\mathrm{sub}}},$$

so a dense oxide of permeability three to four decades below the metal delivers PRF of 10^{2}–10^{3} at micron thickness, *multiplying* the tungsten-limited resistance already present. Recovery is closed by a getter whose hydride-formation free energy ΔG_f sets its equilibrium hydrogen pressure through $p_{\mathrm{eq}}^{\mathrm{getter}} \propto \exp(2\Delta G_f / RT)$: a sufficiently negative ΔG_f makes the getter a hot sink that strips tritium from the stream, and a downstream cold-trap removes it from the carrier at a fixed efficiency η_{ct}. Equations (1)–(13) are the complete formal problem; the remainder of the paper computes their coefficients for Hyperion and reports the solution.

§ 3

Computational methodology: the NVIDIA GPU HPC campaign

CODES AND PROBLEM STATEMENT

The first-wall permeation problem (equations 3–7) was solved with FESTIM [12,13], an open-source finite-element hydrogen-transport code built on the FEniCS finite-element platform [14], run as serial BR-L2-A25 of the Kronos de-risking campaign on the Kronos NVIDIA GPU high-performance-computing fleet (A100/H100/A10-class accelerators). FESTIM discretises the McNabb–Foster mobile/trapped system with continuous Lagrange elements and advances the coupled nonlinearity with a Newton solver; the Sieverts interface condition of equation (5) is enforced through FESTIM's chemical-potential formulation (`chemical_pot`), which transports c_m/S continuously and lets the concentration jump at the tungsten/steel interface. The liquid-metal and barrier screen (BR-SX-03) evaluated the Sieverts driving pressures of equations (11)–(12) and the barrier PRF ladder of equation (13) on the same fleet, and the flowing-lithium divertor thermofluids (HX-16/BR-CX-25) were run alongside; the reference codes for the wider campaign — OpenMC/DAGMC neutronics, SOLPS-ITER edge transport, and plane-wave DFT for the oxide hydrogen-solution energies — are described in the companion neutronics and divertor studies [31,33].

DISCRETISATION, MATERIAL DATA AND MESH

The bilayer was meshed on 573 nodes graded to resolve the implantation layer, the two free surfaces and the tungsten/steel interface, where the concentration gradient and the Sieverts jump are steepest. Material properties were taken from the cited literature rather than fitted: for tungsten, the Frauenfelder diffusivity ($D_0 = 4.1e-7\,m^2/s$, $E_D = 0.390\,eV$) and solubility ($S_0 = 8.88e23\ \mathrm{m^{-3}Pa^{-1/2}}$, $E_S = 1.041\,eV$) [4]; for Eurofer97, the Montupet-Leblond diffusivity ($D_0 = 2.52e-7\,m^2/s$, $E_D = 0.160\,eV$) and solubility ($S_0 = 1.06e23\ \mathrm{m^{-3}Pa^{-1/2}}$, $E_S = 0.27\,eV$), whose fit range 473–$673\,K$ spans the operating wall [6]. The tungsten solubility is extrapolated modestly below its high-temperature fit range, standard practice for this dataset. Figure 3 plots both transport pairs and makes the tungsten-limited character explicit: at 700 K the solubility partition is $S_W/S_E \approx 2.4\times10^{-5}$, three-to-five decades below unity across the whole operating window.

SOLVER, CONVERGENCE AND VERIFICATION

The transient solve diverged near $t \sim 9e4\,s$ under adaptive stepping; because the quantity of interest is the steady permeation flux, the steady-state solve was used and converged in $\sim 25\,s$ of wall time. Convergence was confirmed by mesh refinement at the interface and by monitoring the downstream flux to a fixed tolerance. Verification was performed against the exact analytic two-layer series-resistance solution (equation 9): the finite-element permeation flux matches the analytic diffusion-limited limit to seven significant figures (FESTIM/analytic $= 1.0000000$) on every isothermal case, and the load scaling of equation (8) was verified directly by increasing φ tenfold and recovering a tenfold flux ($1e21 \rightarrow 6.00e15$). A code-to-code cross-check against TMAP8 was attempted but the local TMAP8 binary was unavailable (the MOOSE/PETSc build chain was incomplete); the analytic verification is the same limit the TMAP permeation V&V cases reduce to, and the $\varphi\,R_p/L$ scaling is the standard Anderl/TMAP implantation-driven diffusion-limited result [11,10]. The independence of the loss flux from trap detail (below) makes this verification sufficient for the loss term.

REPRODUCIBILITY OF THE CAMPAIGN

The FESTIM driver, mesh, material-property table and post-processing that produce every permeation number here are archived with the deposit and regenerable end-to-end; the figure-generation script that renders figures 3–9 recomputes the diffusivities, solubilities, breakthrough times and partition ratio from the same constants and reproduces the register anchors (breakthrough $192\,s$ at 600 K, $29\,s$ at 800 K) without hand-tuning. No compute cost or resource pricing is reported here; the campaign is described by its codes, problem scale and verification only.

§ 4

Results

THE PLASMA-FACING LIQUID: LITHIUM OVER TIN

On the fuel-cycle figure of merit of equation (12), the three candidate liquids are separated by orders of magnitude (figure 2, table 1). Pure lithium presents an equilibrium tritium partial pressure about **6.7** decades below tin's and **4.6** decades below lead–lithium's, because lithium chemically binds hydrogen isotopes while tin does not. In loop terms this is a breakthrough buffer of order **7000** h before a lithium loop's tritium works through a protected wall — a margin tin, with its high driving pressure and near-immediate permeation, simply does not have. The same low driving pressure that makes lithium safe for the fuel cycle also makes it the liquid a permeation barrier can most easily protect, since the downstream flux it drives is already small. Lead–lithium keeps its proper role as a breeder/coolant medium rather than the facing liquid. The choice of plasma-facing liquid is lithium.

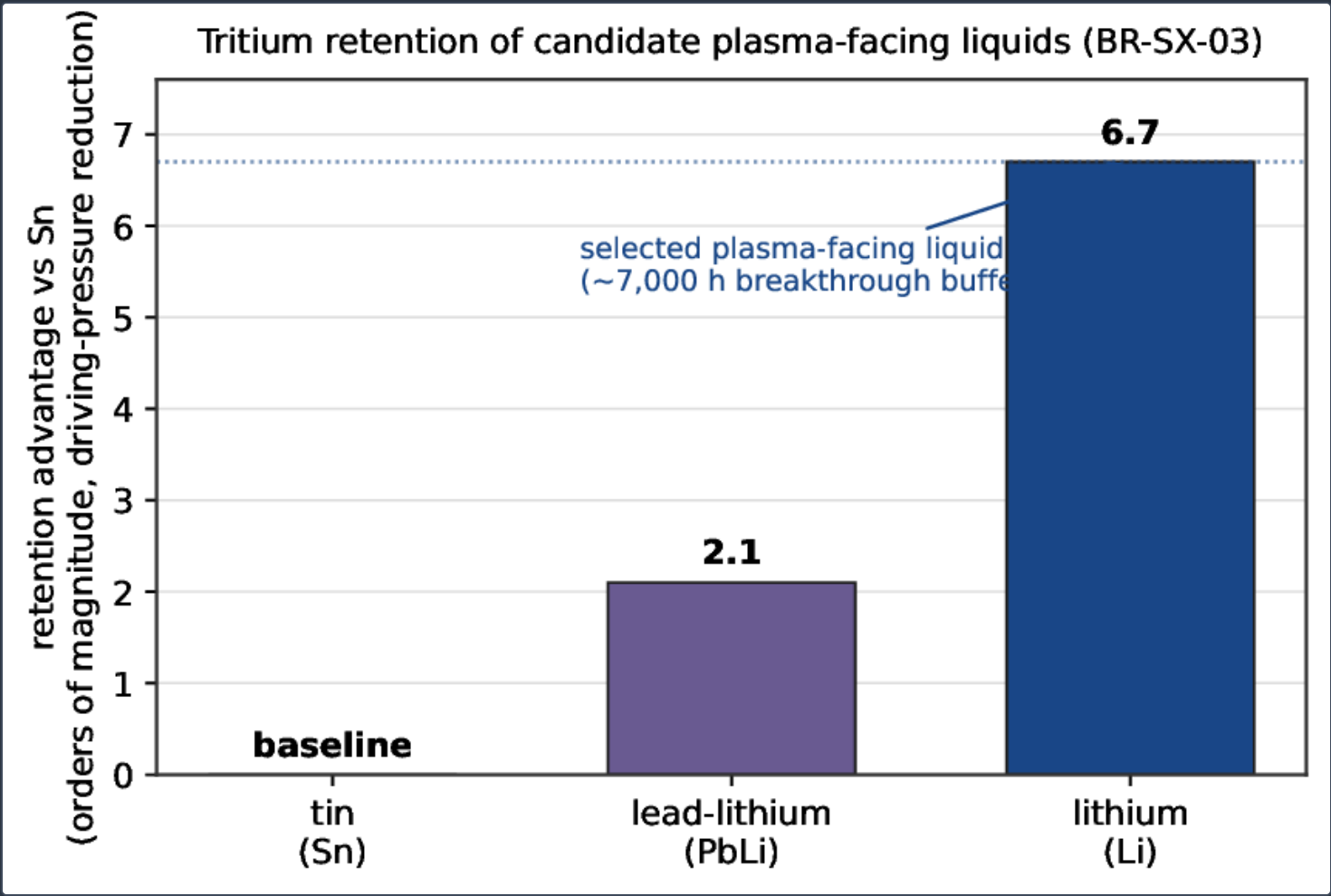

Tritium-retention advantage of the candidate plasma-facing liquids over tin, in decades of equilibrium driving-pressure reduction (equation 12, serial BR-SX-03). Lithium leads by ∼**6.7** orders and is the selected facing liquid; lead–lithium sits ∼**2.1** orders above tin and is retained as a coolant/breeder medium, not the facing liquid.

LIQUID	RETENTION VS SN (ORDERS)	BREAKTHROUGH BUFFER	VERDICT
tin (Sn)	baseline	near-immediate	high driving pressure; rejected
lead–lithium (PbLi)	**~ 2.1**	intermediate	viable coolant/breeder, not the facing liquid
lithium (Li)	**~ 6.7**	**~ 7000 h**	**selected plasma-facing liquid**

Plasma-facing liquid-metal candidates ranked by tritium retention relative to tin. Retention advantage is the reduction in equilibrium tritium driving pressure (equation 12); larger is better for the fuel cycle.

FIRST-WALL PERMEATION IS DIFFUSION-LIMITED AND SMALL

The loss term the fuel cycle actually pays is the tritium that permeates the structure behind the liquid. Solving equations (3)–(7) on the real 0.5 mm W + 2 mm Eurofer stack gives a steady permeation flux of $\mathbf{5.16 \times 10^{14}\ T\,m^{-2}s^{-1}}$ in the operating-gradient case — about $\mathbf{0.082\ g}$ T per square metre per full-power year, only **0.52–0.60 %** of the implanted flux, with **$\sim$99.4 %** re-emitted to the plasma side (table 2). The mechanism is exactly the tungsten-diffusion limit derived in §2: the solubility partition of figure 3 makes tungsten the rate-controlling layer, the steel adds negligible resistance, and the finite-element flux reproduces the analytic two-layer limit to seven significant figures. Figure 4 shows the computed steady mobile-concentration profile: a nearly linear drop across the tungsten armour, a Sieverts partition jump of $\sim \mathbf{2 \times 10^{-5}}$ at the interface, and a shallow gradient across the steel that carries the same flux at much higher concentration.

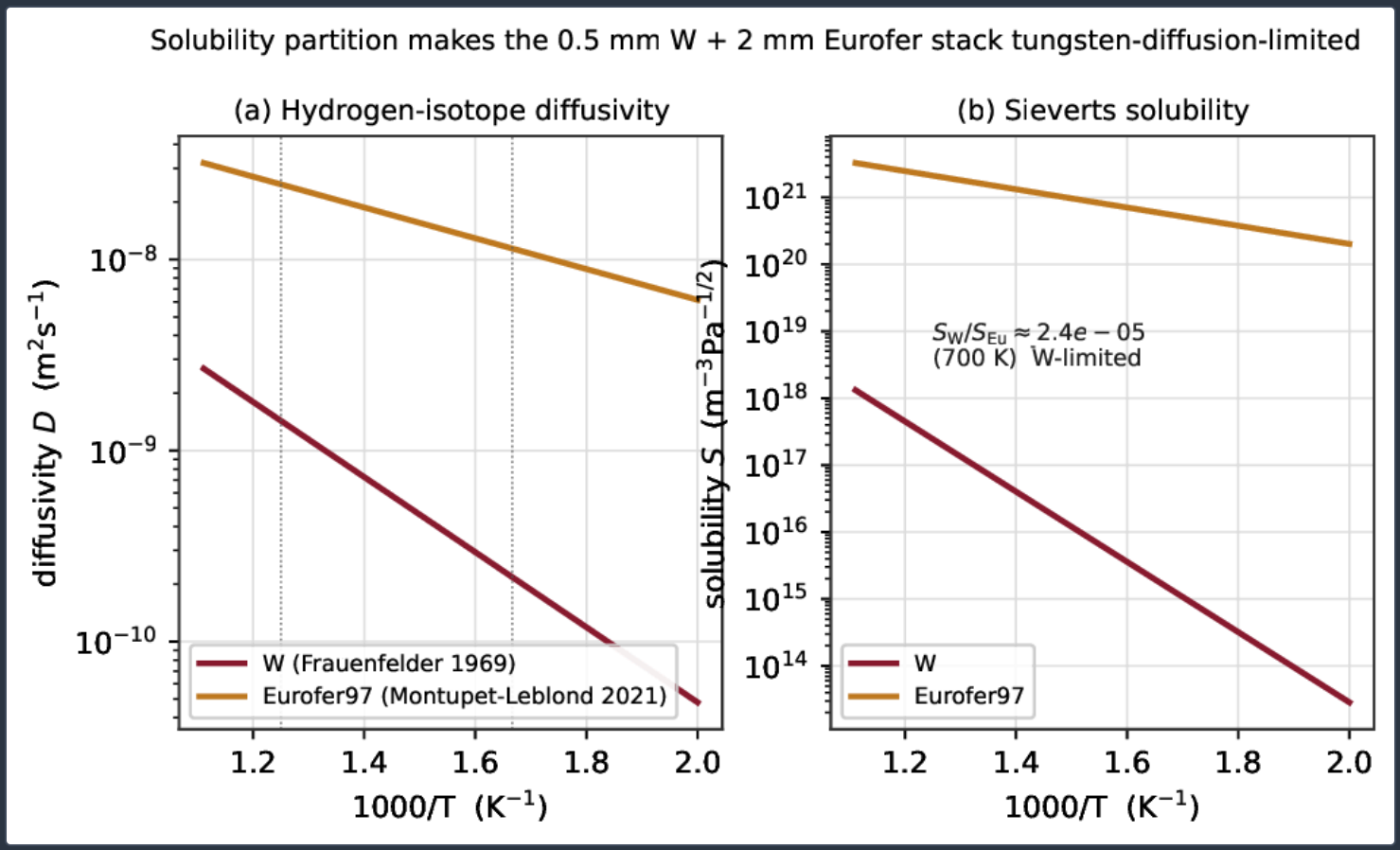

Hydrogen-isotope transport in the two stack materials from the cited data [4,6]: (a) Arrhenius diffusivity and (b) Sieverts solubility for tungsten and Eurofer97 over the operating window. The tungsten solubility carries the larger activation energy, so the interface solubility partition $\mathbf{S_W/S_E \approx 2.4 \times 10^{-5}}$ at 700 K makes the series stack tungsten-diffusion-limited (equation 9). Dotted lines mark the **600** and 800 K bounds.

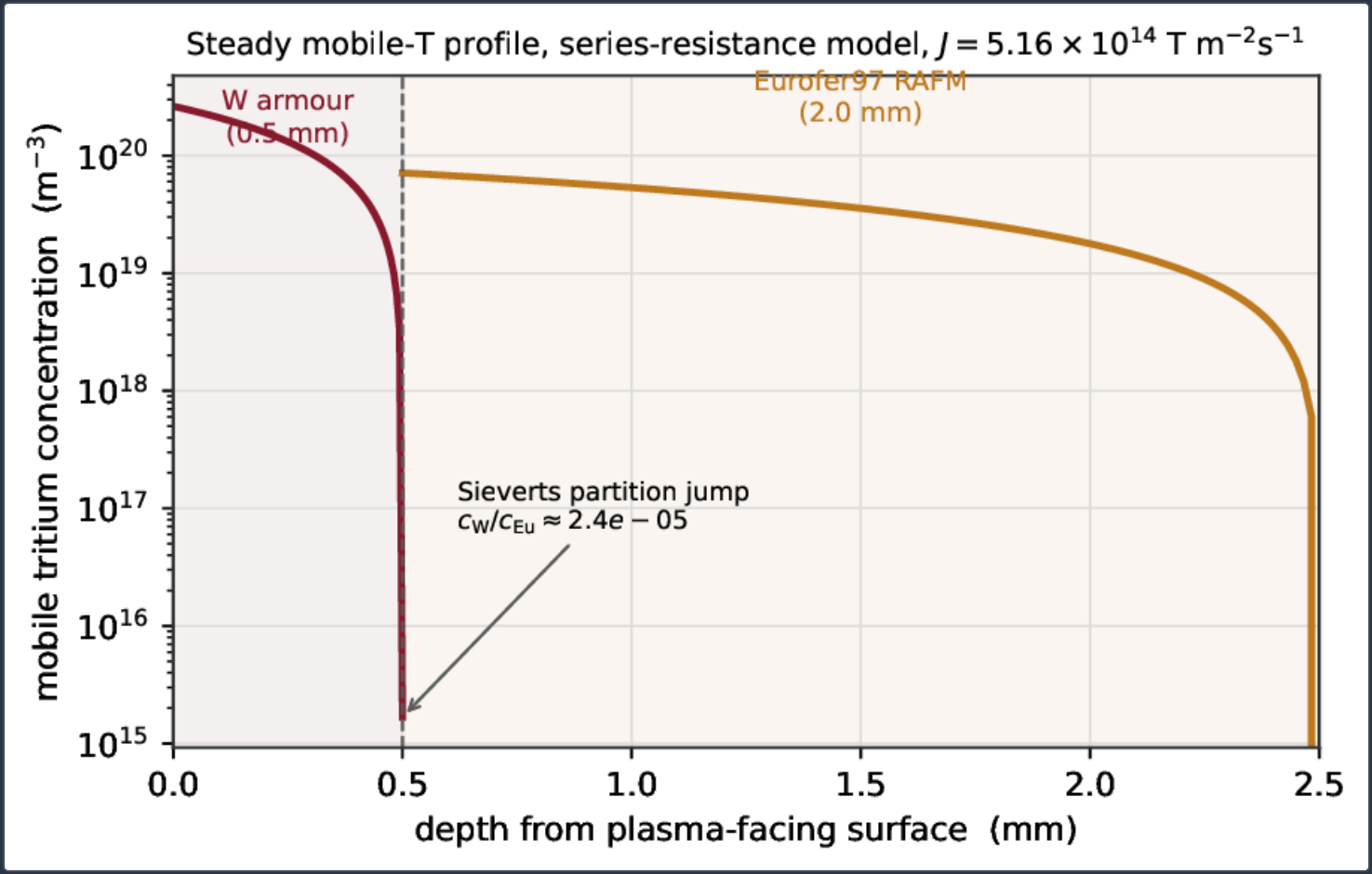

Computed steady mobile-tritium concentration across the bilayer from the two-layer series-resistance model at the operating flux $J = 5.16 \times 10^{14}\ \mathrm{T\,m^{-2}s^{-1}}$. Almost the entire concentration drop is across the tungsten armour; the Sieverts chemical-potential continuity (equation 5) forces a $\sim 2 \times 10^{-5}$ concentration jump at the W/Eurofer interface, above which the steel carries the same flux at far higher concentration and negligible additional resistance.

Because the flux is diffusion-limited, it is temperature-independent and linear in the implanted flux (equation 8): the isothermal cases at **600**, **700** and 800 K all return $6.00 \times 10^{14}\ \mathrm{T\,m^{-2}s^{-1}}$ ($= \varphi\, R_p / L_W$ exactly), and a tenfold rise in φ returns a tenfold flux (figure 5). This is the property that lets the fuel-cycle model of equation (2) carry first-wall permeation as a clean, load-scaled term: for a $\sim 100\ m^2$ first wall the loss is ~ 8–$10\ g$ T per full-power year into structure and coolant, a real but small holdup against a breeder tritium surplus measured in kilograms.

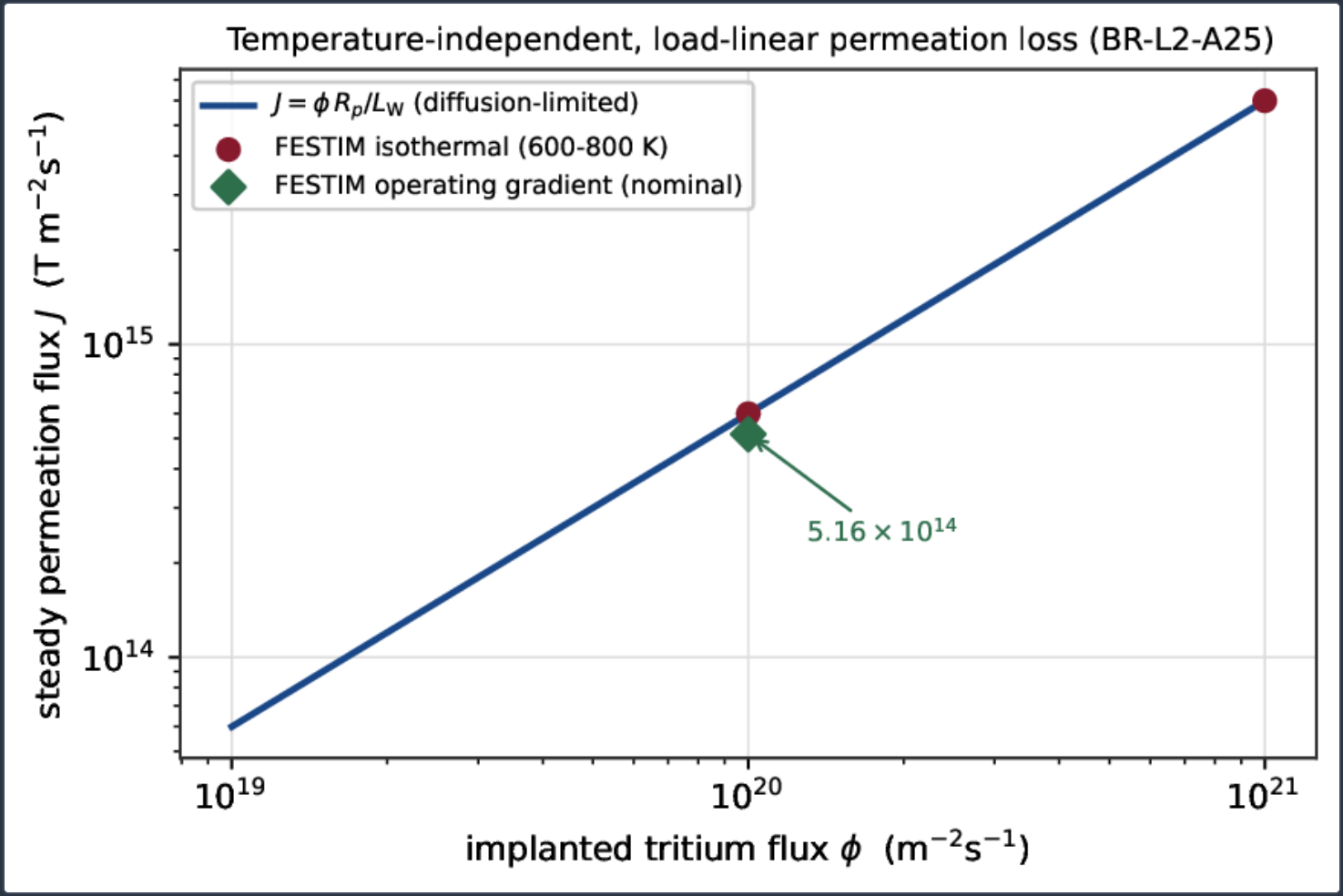

Steady permeation flux versus implanted flux. In the diffusion-limited implantation regime (equation 8) the flux is temperature-independent and linear in load: the finite-element isothermal points at $\varphi = 10^{20}$ and 10^{21} lie on $J = \varphi R_p/L_W$, and the operating-gradient case (5.16×10^{14}) sits just below the isothermal line. Serial BR-L2-A25.

CASE	PERMEATION FLUX (T M^{-2}S^{-1})	RETAINED INVENTORY (T M^{-2})
operating gradient (800→600 K)	5.16×10^{14}	1.75×10^{18} ($\approx 8.8\ \mu$g m^{-2})
isothermal 600 K (worst case)	6.00×10^{14}	8.38×10^{19} (≈ 0.42 mg m^{-2})
isothermal 700 K	6.00×10^{14}	6.2×10^{18}
isothermal 800 K	6.00×10^{14}	9.5×10^{17}

FESTIM first-wall permeation and retained inventory for the §I0.5

RETAINED INVENTORY AND BREAKTHROUGH TIME

The retained wall inventory (mobile plus trapped) is small and hot-wall-favoured (figure 6): $\approx 8.8\ \mu g\,m^{-2}$ on the operating gradient, where the hot tungsten traps are mostly empty, rising to $\approx 0.42\ mg\,m^{-2}$ only in the cold 600 K isothermal bound, and falling to $9.5 \times 10^{17}\ T\,m^{-2}$ at 800 K. The inventory is tungsten-dominated (the 1.00 eV trap). The transient is short: the analytic breakthrough time of equation (10), evaluated with the tungsten diffusivity, is $192\ s$ at 600 K and $29\ s$ at 800 K (figure 7), so permeation reaches steady within minutes of a burn start and holds no surprise transient. Loss flux and inventory are cleanly separated: the flux is set by geometry and load, the inventory by trap population and temperature.

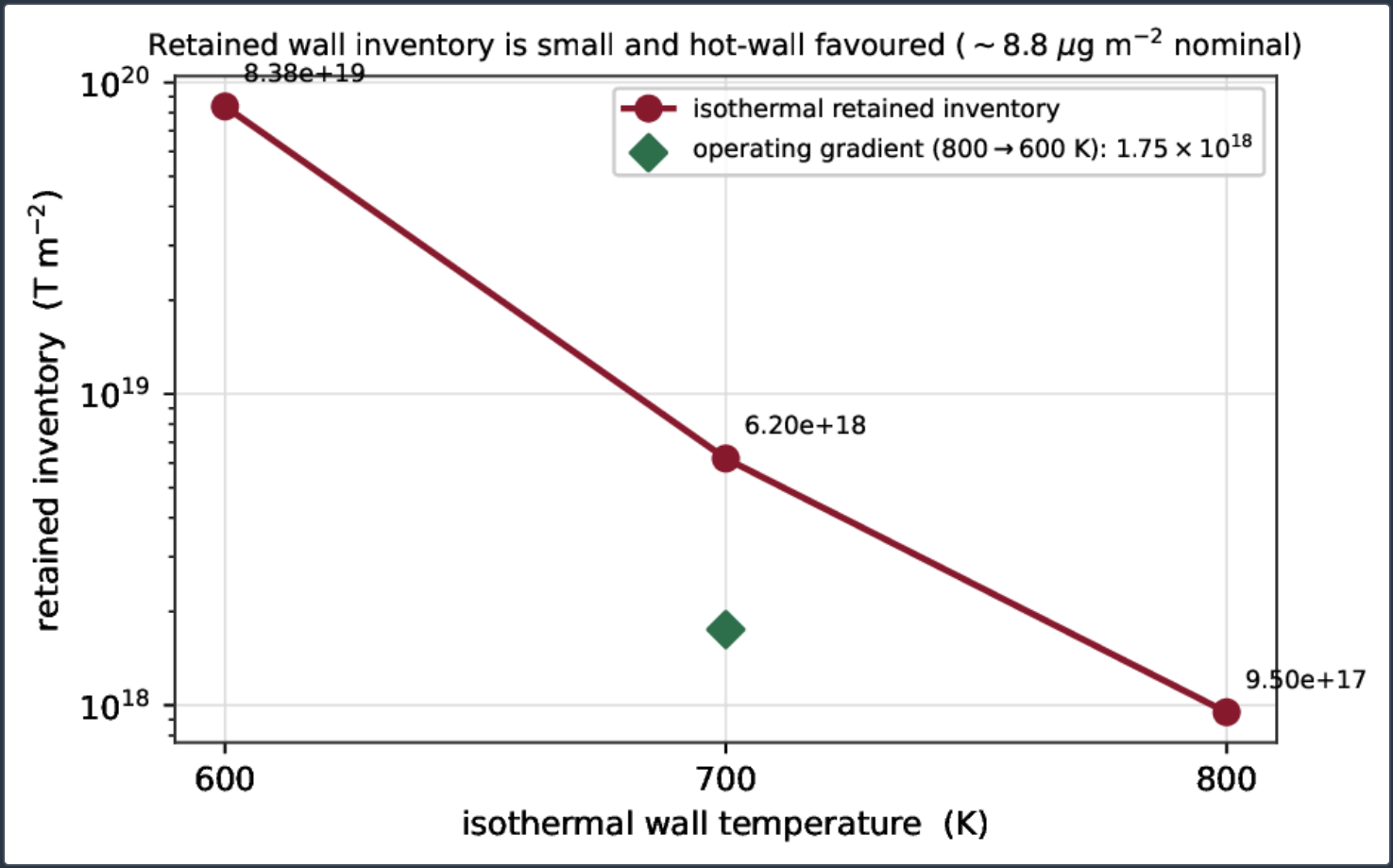

Retained tritium inventory versus wall temperature (serial BR-L2-A25). The inventory is hot-wall favoured — highest in the cold 600 K isothermal bound, lowest at 800 K — and the operating gradient case ($1.75 \times 10^{18}\ T\,m^{-2} \approx 8.8\ \mu g\,m^{-2}$) sits near the hot end. The diffusion-limited loss flux is unchanged across all four cases.

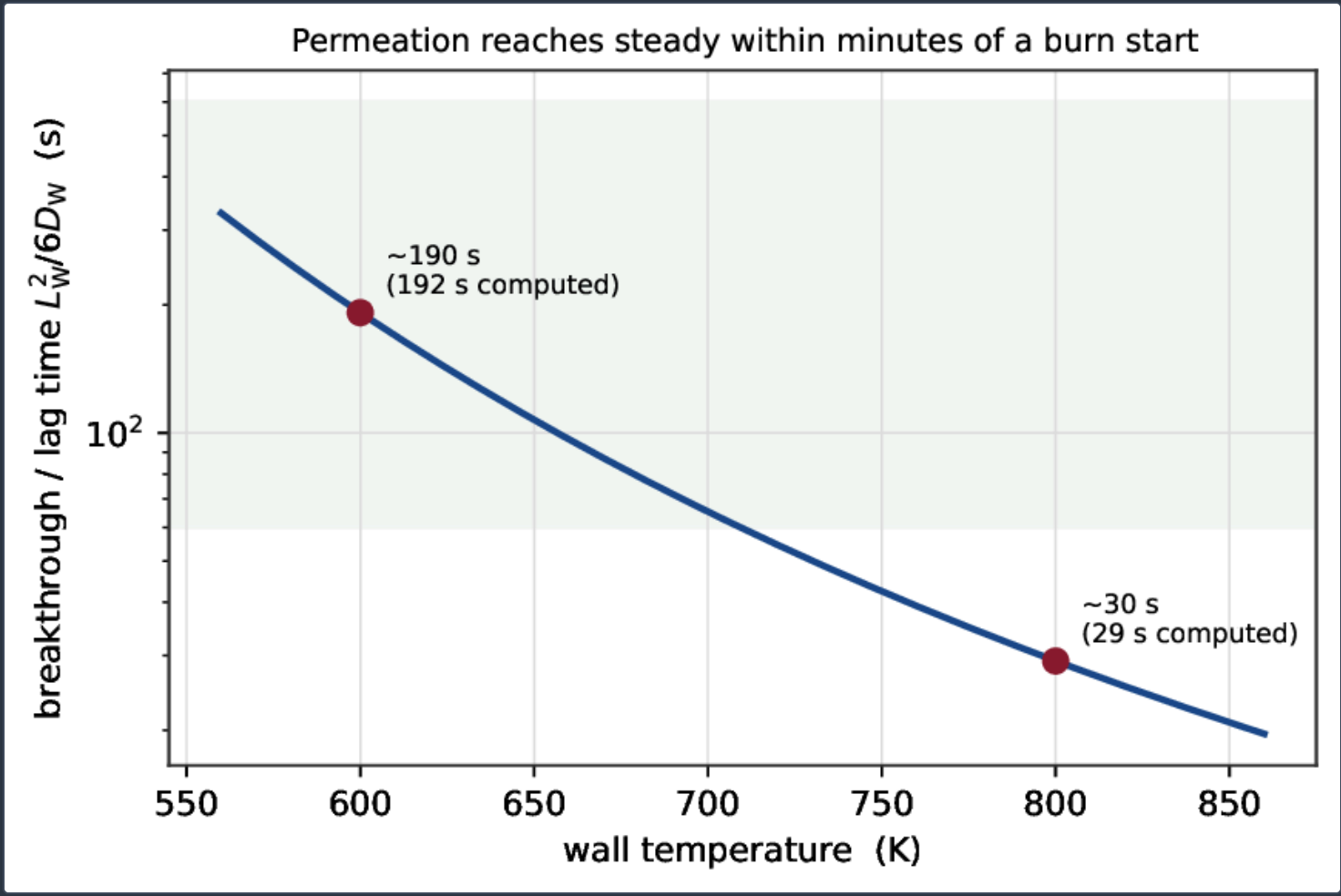

Breakthrough (time-lag) time $\tau = L_W^2/6D_W$ of the rate-controlling tungsten armour versus temperature (equation 10). The computed curve passes through the register anchors of $\sim 190\ s$ at 600 K and $\sim 30\ s$ at 800 K; permeation is at steady within minutes of a burn start.

BARRIER LADDER AND CLOSING THE RECOVERY LOOP

Even a sub-percent permeation loss is worth cutting when the coating is cheap in neutronic and thermal terms, and the standalone fuel-cycle target for Hyperion (BR-SX-17) is a permeation-reduction factor of order **2000**. A PRF screen (equation 13) ranks the candidate barriers $\mathbf{Al_2O_3}$ **(PRF** $\sim 10^3$**)** $>$ $\mathbf{Er_2O_3}$ **(**$\sim 3 \times 10^2$**)** $>$ **TiC** $>$ **TiN** (figure 8). Alumina and erbia are the standard fusion barrier oxides for good reason: a dense, adherent oxide is a low-permeability series layer that *multiplies* the tungsten-limited resistance already established, so the barrier and the diffusion limit act in series rather than in competition. No single oxide reaches PRF $\sim$**2000** alone, but stacked on the tungsten-limited baseline the combination clears the requirement. Recovery is closed by an yttrium hot-trap, whose hydride formation free energy of $\Delta G = -83$ to $-97\ kJ/mol$ makes it a hot sink that getters tritium from the lithium stream, and a downstream cold-trap that removes it at **92 %** efficiency. Retention (barrier) and recovery (getter train) together turn the first-wall tritium budget into a closed, accountable circuit — what little permeates is caught, and what is caught is measured — which is what the real-time tritium-accountancy twin [30] carries as a bounded holdup.

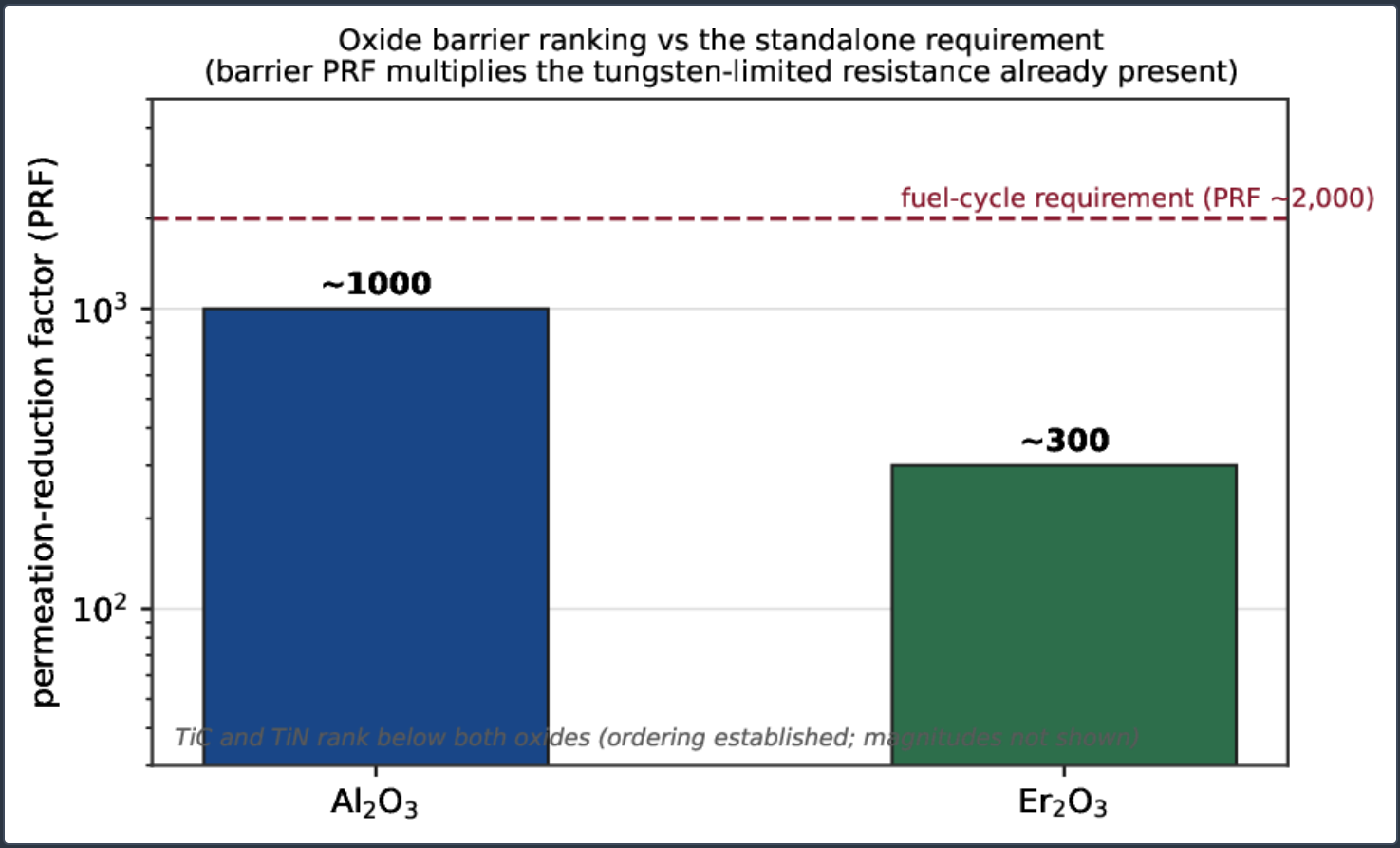

Measured permeation-reduction factors of the two leading oxide barriers (serial BR-SX-03) against the standalone fuel-cycle requirement of PRF $\sim$**2000** (serial BR-SX-17). Neither oxide reaches the requirement alone, but each multiplies the tungsten-limited resistance already present (equation 13); TiC and TiN rank below both oxides. Logarithmic axis.

DIVERTOR INTEGRATION: THE EXHAUST CO-BENEFIT

The lithium choice pays a second dividend at the exhaust. A flowing-lithium film divertor handles a surface heat flux of **2.8**, **4.9** and **6.7** MW/m^2 at film velocities of **2**, **5** and 10 m/s respectively (figure 9, HX-16), the limit set by the evaporation (surface-temperature) ceiling, which suits the detached-operation regime the breeder runs. A lithium vapour shield self-limits its surface near **869** $^\circ C$ at 8 MW/m^2 (BR-CX-25), adding a passive margin at the strike point. The same lithium loop that protects the fuel cycle at the first wall therefore also carries in-loop tritium recovery as a co-benefit and provides a self-healing exhaust surface — one material choice serving three functions — and it is the basis of the companion flowing-lithium vapour-box divertor with in-loop tritium extraction [31].

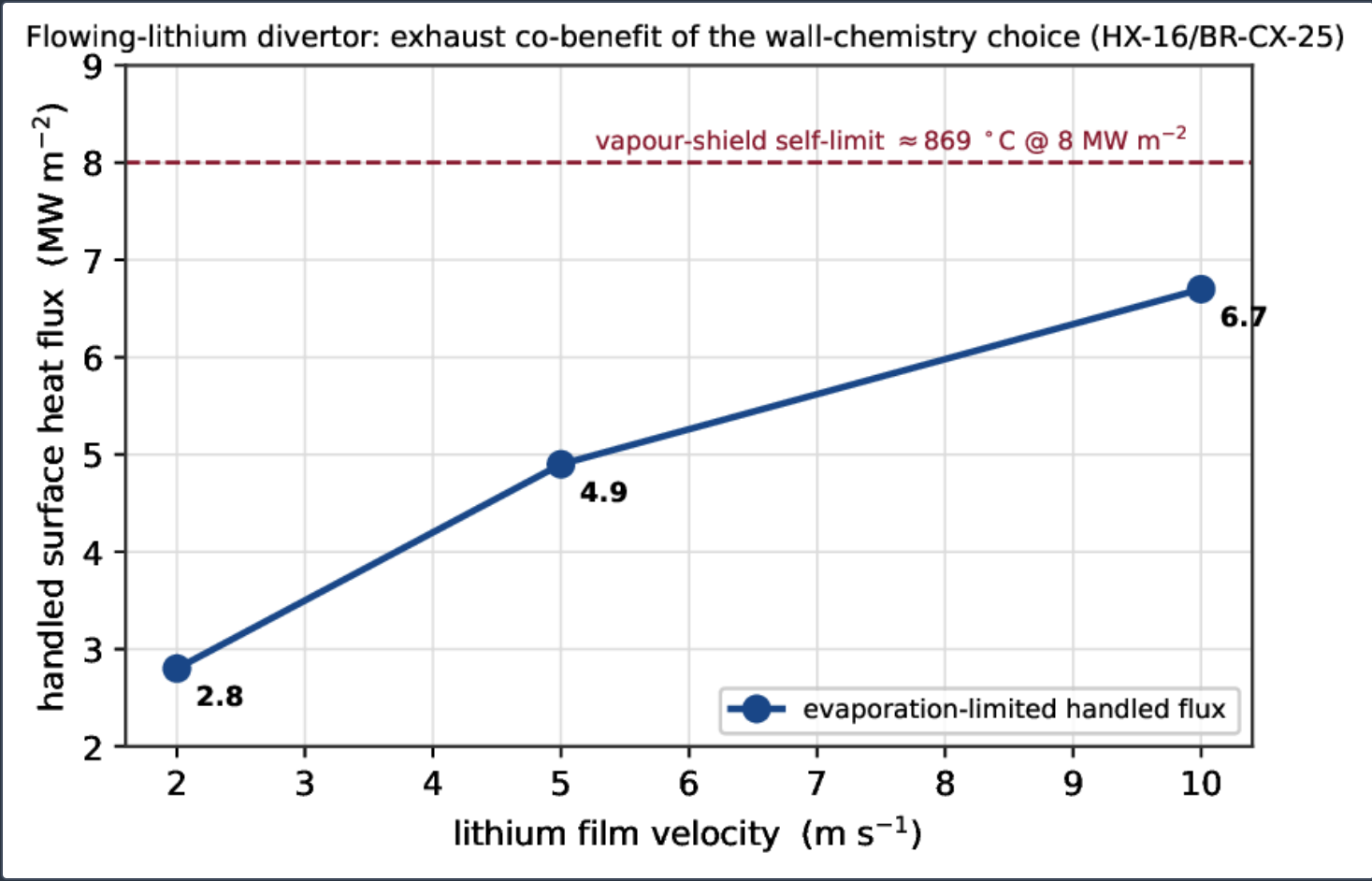

Evaporation-limited handled heat flux of the flowing-lithium film divertor versus film velocity (serial HX-16): **2.8**, **4.9** and **6.7** MW/m^2 at **2**, **5** and 10 m/s. The dashed line marks the vapour-shield self-limit (≈ **869** $^\circ C$ at 8 MW/m^2, BR-CX-25). The wall-chemistry choice that protects the fuel cycle also carries the exhaust.

§ 5

Discussion

THE TWO DECISIONS REINFORCE EACH OTHER

The two first-wall decisions are not independent trades but a single coherent choice. Lithium's low tritium driving pressure (equation 11) is simultaneously what makes it the safe plasma-facing liquid and what makes it the liquid a barrier protects most easily, because the downstream flux it drives is already small. The tungsten-diffusion-limited stack (equation 9, figures 3–4) holds the baseline permeation loss under a percent of the implanted flux before any coating is applied. The alumina/erbia barrier plus yttrium getter train drives the residual loss down and routes it into a measured recovery stream. Tin is excluded on the one axis that matters, and lead–lithium keeps its proper role. The result is that first-wall permeation enters the self-sufficiency condition of equation (2) as a bounded, well-characterised term rather than an open risk.

QUANTITATIVE COMPARISON WITH PUBLISHED BENCHMARKS

The permeation number is consistent with, and more sharply bounded than, the fusion permeation literature. The tungsten-diffusion-limited character follows directly from the Frauenfelder solubility being three-to-five decades below Eurofer's over the operating window [4,6], exactly the partition that measured permeation experiments on aluminised and oxide-coated steels invoke to explain their PRF [7,16]. The diffusion-limited, temperature-independent, load-linear flux (equation 8, figure 5) is the standard Pick–Sonnenberg/Anderl implantation-driven result [10,11], and recovering the analytic two-layer limit to seven significant figures places the finite-element solve firmly inside the verified TMAP permeation V&V family. The barrier ranking — $\mathrm{Al_2O_3} \sim 10^{3}$, $\mathrm{Er_2O_3} \sim 3 \times 10^{2}$ — sits within the 10^{2}–10^{4} band reported for dense oxide permeation barriers [15,17,19,18]. On the liquid side, the choice of lithium as a low-recycling, tritium-retaining plasma-facing material is consistent with the CDX-U/LTX/NSTX experience [20,21] and with the analyses that reserve tin and tin–lithium for cases where lithium's tritium inventory is judged unacceptable [23,24]; here that inventory is precisely the property that protects the fuel cycle. Finally, treating first-wall permeation as a sub-percent, kilogram-margin loss term is what the global D–T self-sufficiency analyses require of a credible breeder [1,3], and it feeds the Hyperion tritium breeding ladder [29] and accountancy twin [30] directly.

CONSISTENCY WITH THE HYPERION DESIGN POINT

Nothing in the first-wall architecture conflicts with the frozen machine. The 0.5 mm tungsten armour and 2 mm Eurofer wall are the same stack the RAFM-steel qualification [32] and the first-wall neutron-damage lifetime study [33] carry, and the flowing-lithium exhaust is the same loop the divertor study [31] develops. The breeder operates at $P_{\mathrm{fus}} = 85.04\,MW$, $I_p = 9.66\,MA$, $Q = 3.076$, $\delta = -0.30$, $B_0 = 8\,T$ behind a centrepost peak field of 16.84 T; the permeation loss is a platform-level fuel-cycle number, not a function of these plasma parameters beyond the implanted flux φ that sets its scale.

§ 6

Limitations

The single open item is the barrier ranking. It is drawn here from established permeation-reduction data and oxide chemistry rather than computed from theory; the first-principles DFT hydrogen-solution energies for the $\mathbf{Al_2O_3}$ and $\mathbf{Er_2O_3}$ barriers, which would set their PRF from $\boldsymbol{E_{\mathrm{sol}}(\mathrm{H})}$ rather than from measured factors, were not completed (the local MPI build was blocked) and are queued on the NVIDIA GPU HPC campaign. The permeation loss term itself is robust to this: being diffusion-limited it is unaffected by trap detail, and neutron-damage traps — omitted here — can only raise the retained inventory (by an estimated factor of $\mathbf{10–100}$), never the steady loss flux, which they merely delay. The retained-inventory numbers are therefore a clean-material lower bound, while the loss flux stands as computed. Two secondary conservatisms bracket the flux the safe way: the absence of a front recombination barrier places the permeation on the conservative-high side, and a thicker armour would lower it in proportion to $\boldsymbol{1/L_{\mathrm{W}}}$.

§ 7

Conclusion

Lithium is the plasma-facing liquid for a compact spherical-tokamak breeder. It retains tritium some $\mathbf{6.7}$ orders of magnitude more strongly than tin — closing off the dominant fuel-cycle hazard through the low equilibrium driving pressure of equation (11) — and it hands the exhaust a $\mathbf{2.8–6.7}\ \boldsymbol{MW/m^2}$ flowing-film surface as a bonus. Behind it, the real 0.5 mm W + 2 mm Eurofer stack leaks only $\mathbf{0.082}\ \boldsymbol{g}$ T m $^{\mathbf{-2}}$fpy$^{\mathbf{-1}}$ — a computed, not assumed, number: tungsten-diffusion-limited, temperature-independent, load-linear, and matching the analytic two-layer limit to seven significant figures. An $\mathbf{Al_2O_3/Er_2O_3}$ barrier and an yttrium getter train close the recovery loop into a measured circuit. Together these choices make the first-wall tritium budget a small, bounded and accountable term in the self-sufficiency condition $\boldsymbol{\Lambda = \mathrm{TBR}(1-\varepsilon) - 1 \geq 0}$, and they do so with a single material choice that protects the fuel cycle, admits a barrier, and self-heals the exhaust at once.

Acknowledgments tocsectionAcknowledgments Part of the Kronos Fusion Energy 2026 design series. The authors thank the Kronos physics de-risking programme for the frozen result set underlying every quantitative claim, and the NVIDIA GPU high-performance-computing campaign that produced the finite-element permeation solve.

Reproducibility. The permeation and inventory numbers are frozen results (serial BR-L2-A25, FESTIM) in the Kronos Physics De-Risking Register [34], regenerable from the archived FESTIM driver, mesh and material-property table; the liquid-metal retention and barrier ranking are the M3 materials-chemistry gate (serial BR-SX-03), and the divertor thermofluids are HX-16/BR-CX-25. The figure-generation script deposited with this paper recomputes the transport coefficients, breakthrough times and solubility partition from the cited constants and reproduces the register anchors. This paper is archived at its DOI doi:10.5281/zenodo.22645870; official version: https://www.kronosfusionenergy.com/publications/tritium-permeation-barrier-coatings-for-a-compact-spher.html and its official page https://www.kronosfusionenergy.com/publications/tritium-permeation-barrier-coatings-for-a-compact-spher.html; the series register is doi:10.5281/zenodo.22133057.

Data availability tocsectionData availability The FESTIM inputs and permeation/inventory outputs, the liquid-metal and barrier screen, and the figure-generation script for figures 2–9 are archived with the deposit at doi:10.5281/zenodo.22645870, which references the Kronos 2026 series register doi:10.5281/zenodo.22133057. Any economic analysis is reported separately and is not part of the public deposit.

Competing interests tocsectionCompeting interests Provisional patent applications relating to aspects of this work have been filed.

tocsectionReferences

Portfolio, People & Record

The intellectual-property estate, the people who built it, the limitations that gate it, and the sources it rests on.

1	4	40	27
GRANTED PATENT	2026 PROVISIONALS	TEAM MEMBERS	2022 PROVISIONALS

INTELLECTUAL PROPERTY

The patent portfolio

The estate spans a granted high-field magnet patent, pending utility and 2026 provisional filings that map to the two products, a digital-twin control provisional, a registered trademark application, and the original 2022 provisional family. Every patentable disclosure in the five-paper arXiv drop was protected **before** publication: the breeder and burner provisionals were filed 1–2 August, and a publication-gap omnibus filing the evening before the drop swept up the DEC, plasma-control, and REBCO-winding matter of the three otherwise-unprotected papers. Patent numbers and application serials are matters of public record; claim scope is summarised, not reproduced.

GRANTED & PENDING UTILITY

US 12,009,112	High-field tilted graded-REBCO magnet architecture (KRONO-002A) · *app. 17/878,550*	GRANTED
US 17/878,507	Core device / method (KRONO-001A) · *utility*	PENDING

2026 PROVISIONAL FILINGS — MAPPED TO THE PRODUCTS

64/124,209	Hyperion — spherical-tokamak tritium / helium-3 foundry · *breeder · filed Aug 2026*	FILED
64/124,220	Aegis / MetroVolt — synchrotron-cutoff, fuel-selection & plug-winding · *generator · filed Aug 2026*	FILED
64/115,167	KRONOS-CTRL digital-twin plant control · *provisional · filed Jul 2026*	FILED
64/005,440	Integrated spherical-tokamak fusion architecture · *early integrated-architecture filing · filed Mar 2026*	FILED
64/105,530	Negative-triangularity spherical-tokamak architecture · *foundational ST filing · filed Jul 2026*	FILED
64/128,097	Publication-gap omnibus — quasineutral two-species expander DEC · provenance-gated / latency-split plasma control · as-built high-field winding & conductor architecture · *filed 7 Aug 2026, the evening before the arXiv drop*	FILED

TRADEMARK & ORIGIN

FTK-98801894	Kronos Fusion Energy — trademark application	FILED
KR-2022-*	Original provisional family (KR-2022-00001 … 00027) · *27 filings, 2022*	PRIORITY

The narrow, defensible magnet novelty — the specific conductor and the digital-twin winding optimisation, not high-field REBCO as a category — is the commercial core that can earn ahead of any Q > 1 milestone, with markets in fusion magnet supply, MRI/NMR, accelerators, and proton therapy. The claim is scoped honestly: the high field is a *system field* result, not a stand-alone-coil record; the small-bore plug coil is structurally infeasible as a bare winding but resolved by a stress-managed structural shield (feasible-pending-FEA); and the winding-tape experiment returned a *null result*. The value is the method, not a field record.

THE TEAM

Founding partners, board, advisors & auditors

Kronos is built by a bench of advanced-fuel-fusion, high-field-magnet, direct-conversion, and materials specialists, with a board and operations team drawn from defense, national laboratories, and industry. Dates are shown as ranges; where a tenure has ended or is term-ending, the range says so.

FOUNDING PARTNERS — SCIENCE

Dr. Gerald Kulcinski
Co-Founder · Helium-3 & Advanced-Fuel Fusion
UW–Madison · 2023–Present

Dr. Carl Weggel
Chief Scientist / S.M.A.R.T. Design
MIT Alcator Program · 2022–Present

Dr. Robert J. Weggel
Magnetic Field Design
MIT Magnet Lab · 2022–Present

BOARD

Priyanca Ford
Founder & CEO · Executive Board
2022–Present

Bandel Carano
Finance / Strategy
Oak Investment Partners / Stanford · 2025–2026

Patrick Schweiger
Fusion Device Engineering
Oklo / CFS / TerraPower · 2025–Present

SCIENTIFIC ADVISORS

Dr. Steven O. Dean
Fusion Policy & History
DOE / Fusion Power Associates · 2025–Present

Dr. Patrick H. Diamond
Plasma Turbulence & Transport
UC San Diego · 2025–Present

Dr. Jack J. Dongarra
HPC & Numerical Algorithms
Turing Award · 2025–Present

Dr. Nasr M. Ghoniem
Chief Material Scientist
UCLA · 2025–Present

Dr. Siegfried Glenzer
Plasma Physics & Laser Fusion
Stanford / SLAC · 2022–Present

Dr. David A. Hammer
Pulsed-Power Fusion
Cornell · 2025–Present

Dr. Donald A. Spong
Plasma Theory & Confinement
ORNL · 2025–Present

Dr. Curtis Smith
Risk Assessment & Nuclear PRA
MIT / Idaho National Lab · 2025–Present

RADM (Ret.) David Goggins
Naval Engineering & Power-Plant Design
U.S. Navy · 2023–2026

Dr. Konstantin Batygin
Mathematician
Caltech · 2022–2025

Dr. Ruben Fair
Magnet Design / ITER Liaison
PPPL / Jefferson Lab · 2022–2025

Dr. Paul S. Weiss
Materials & Nanotechnology
UCLA · 2022–2025

SCIENTIFIC AUDITORS

Dr. Wilfred A. Cooper
Plasma Equilibrium Theory
EPFL / Swiss Plasma Center · 2025–Present

Dr. Ahmed Hassanein
Plasma–Material Interactions
Purdue / Argonne · 2025–Present

Dr. Patrick E. Hopkins
Extreme Thermal Materials
U. of Virginia · 2025–Present

Dr. Peter Hosemann
Materials Joining & Structural Integrity
UC Berkeley · 2025–Present

Dr. Travis W. Knight
Advanced Nuclear Fuels & Systems
U. of South Carolina · 2025–Present

Dr. Philippe Lebrun
Cryogenics & Magnet Cooling
CERN · 2025–Present

Dr. Nitendra Singh
Nuclear Safety & Fuel Cycle
ITER · 2025–Present

Dr. Guido Van Oost
Magnetic Confinement & Fusion Systems
Ghent University · 2025–Present

Dr. Gary S. Was
Radiation Materials & Structural Integrity
U. of Michigan · 2025–Present

Dr. Ray Sedwick
Direct Energy Conversion
U. of Maryland · 2025

OPERATIONS

Michael Laughlin
Chief Operating Officer
2022–Present

Martin Owens
Chief Strategy Officer
LANL / GE Hitachi · 2022–Present

MG (Ret.) Paul Pardew
Chief Contracting Officer
Army Contracting Command · 2022–Present

David Beck
Fusion Commercialization
U.S. Space Force · 2024–Present

Sushma Bhatia
Environmental & Legislative
Google · 2022–Present

Michael De Frenza
Technology Licensing
2023–Present

MG (Ret.) Robin L. Fontes
Cybersecurity & Defense
Army Cyber Command · 2022–Present

Vijay Gehani
Supply Chain & Components
INOX India · 2024–Present

Jon Michel Greenwood
IT & AI Infrastructure
Live Nation · 2023–Present

Brian C. O'Neill
National Security
CIA / ODNI · 2022–Present

Gen. (Ret.) Gustave F. Perna
DoD Liaison
Operation Warp Speed · 2022–2023

Andrea Romero
Marketing Lead
2022–Present

Legal counsel is retained; those roles are held on the internal roster and are not listed here.

SOURCES

References

1 M Abdou *et al*, Physics and technology considerations for the deuterium–tritium fuel cycle and conditions for tritium fuel self sufficiency, *Nucl. Fusion* **61** 013001 (2021).

2 M A Abdou *et al*, Deuterium–tritium fuel self-sufficiency in fusion reactors, *Fusion Technol.* **9** 250 (1986).

3 M E Sawan and M A Abdou, Physics and technology conditions for attaining tritium self-sufficiency for the DT fuel cycle, *Fusion Eng. Des.* **81** 1131 (2006).

4 R Frauenfelder, Solution and diffusion of hydrogen in tungsten, *J. Vac. Sci. Technol.* **6** 388 (1969).

5 A McNabb and P K Foster, A new analysis of the diffusion of hydrogen in iron and ferritic steels, *Trans. Metall. Soc. AIME* **227** 618 (1963).

6 F Montupet-Leblond *et al*, Permeation and trapping of hydrogen in Eurofer97, *Nucl. Mater. Energy* **29** 101062 (2021).

7 G A Esteban *et al*, Hydrogen isotope diffusive transport parameters in reduced activating martensitic steel Eurofer′97, *J. Nucl. Mater.* **367–370** 473 (2007).

8 O V Ogorodnikova, J Roth and M Mayer, Deuterium retention in tungsten in dependence of the surface conditions, *J. Nucl. Mater.* **313–316** 469 (2003).

9 J Roth *et al*, Recent analysis of key plasma wall interactions issues for ITER, *J. Nucl. Mater.* **390–391** 1 (2009).

10 M A Pick and K Sonnenberg, A model for atomic hydrogen–metal interactions — application to recycling, recombination and permeation, *J. Nucl. Mater.* **131** 208 (1985).

11 G R Longhurst, *TMAP7 User Manual*, Idaho National Laboratory report INL/EXT-04-02352 (2008).

12 R Delaporte-Mathurin, E A Hodille, J Mougenot, Y Charles and C Grisolia, Finite element analysis of hydrogen retention in ITER plasma facing components using FESTIM, *Nucl. Mater. Energy* **21** 100709 (2019).

13 R Delaporte-Mathurin *et al*, FESTIM: an open-source code for hydrogen transport simulations, *J. Open Source Softw.* (2024).

14 M S Alns *et al*, The FEniCS Project Version 1.5, *Arch. Numer. Softw.* **3** 100 (2015).

15 R A Causey, R A Karnesky and C San Marchi, Tritium barriers and tritium diffusion in fusion reactors, in *Comprehensive Nuclear Materials* (Elsevier) vol. 4, p. 511 (2012).

16 D Levchuk *et al*, Deuterium permeation through Eurofer and α-alumina coated Eurofer, *J. Nucl. Mater.* **328** 103 (2004).

17 A Aiello, A Ciampichetti and G Benamati, An overview on tritium permeation barrier development for WCLL blanket concept, *J. Nucl. Mater.* **329–333** 1398 (2004).

18 K S Forcey, D K Ross and C H Wu, The formation of hydrogen permeation barriers on steels by aluminising, *J. Nucl. Mater.* **182** 36 (1991).

19 G W Hollenberg, E P Simonen, G Kalinin and A Terlain, Tritium/hydrogen barrier development, *Fusion Eng. Des.* **28** 190 (1995).

20 R Kaita *et al*, Low recycling and high power density handling physics in the Current Drive Experiment-Upgrade with lithium plasma-facing components, *Phys. Plasmas* **14** 056111 (2007).

21 M A Jaworski *et al*, Liquid lithium divertor characteristics and plasma–material interactions in NSTX high-performance plasmas, *Nucl. Fusion* **53** 083032 (2013).

22 R J Goldston, R Myers and J Schwartz, The lithium vapor-box divertor, *Phys. Scr.* **T167** 014017 (2016).

23 J W Coenen *et al*, Liquid metals as alternative solution for the power exhaust of future fusion devices: status and perspective, *Phys. Scr.* **T159** 014037 (2014).

24 R E Nygren and F L Tabar\′es, Liquid surfaces for fusion plasma facing components — a critical review. Part I: physics and PSI, *Nucl. Mater. Energy* **9** 6 (2016).

25 J E Menard *et al*, Fusion nuclear science facilities and pilot plants based on the spherical tokamak, *Nucl. Fusion* **56** 106023 (2016).

26 B N Sorbom *et al*, ARC: a compact, high-field, fusion nuclear science facility and demonstration power plant with demountable

COLOPHON

How this document was made

The Kronos Fleet — Combined Editorial, 2026 is set in **Fraunces** (display), **Gelasio** (text), and **IBM Plex Mono** (data & equations), carried forward from the Kronos editorial design system.

The figures are rendered at 300 dpi from the deposited generator scripts; the document is composed as a single self-contained file with embedded fonts and imagery, paginated to US Letter, and rendered to PDF through a headless Chromium engine in matched light and dark editions.

Every headline quantity carries an evidence class; withdrawn and restated values are marked as such. Nothing herein is frozen beyond the founder-approved Tier-A set.

Explore it live — turn the interactive 3-D model, run the deposited solvers in the physics validator, and watch the companion film series.

◆

LEGAL NOTICE

Notice, status, and distribution

Conceptual design & simulation study. This document reports a conceptual design and simulation study. It is not a construction commitment, a safety-analysis report, a regulatory filing, or an offer of securities. Forward-looking statements — schedules, costs, market sizes, and performance — are estimates subject to the limitations set out in the Simulations part and may change.

Numbers and their classes. Quantities are reported with evidence classes and case labels; modelled, assumed, and requirement-class values are identified as such and are not to be quoted without their labels.

Public edition. This edition carries the physics and design only; all financial, funding, and defense-commercial content has been removed for public distribution. The scientific text corresponds to the arXiv and journal submissions.

THE 2026 KRONOS SERIES

One programme, many papers

This editorial is one paper in the Kronos 2026 series — a real fusion company's complete, reproducible physics record for a spherical-tokamak breeder and its low-neutron D–^{3}He tandem-mirror burners. Every headline number is a frozen anchor in the Physics De-Risking Register.

Explore the whole programme: the De-Risking Register, the interactive 3-D model, and the physics validator.

KRONOS FUSION ENERGY

Tritium Permeation-Barrier Coatings for a Compact Spherical-Tokamak Breeder: The Liquid-Lithium-over-Tin Wall-Chemistry Choice

A real fusion company building real machines. Explore the science, live.

Zenodo · doi:10.5281/zenodo.22645870

Read on kronosfusionenergy.com

The Physics De-Risking Register